4540 Vol. 48, No. 17 / 1 September 2023 / Optics Letters Letter

Optics Letters

# Ultra-linear broadband optical frequency sweep for a long-range and centimeter-spatial-resolution OFDR

HUAJIAN ZHONG,[1,2] CAILING FU,[1,2,*] PENGFEI LI,[1,2] BIN DU,[1,2] CHAO DU,[1,2] YANJIE MENG,[1,2] XIAOYU YIN,[1,2] CHANGRUI LIAO,[1,2] AND YIPING WANG[1,2,3]

[1]Shenzhen Key Laboratory of Photonic Devices and Sensing Systems for Internet of Things, Guangdong and Hong Kong Joint Research Centre for Optical Fibre Sensors, State Key Laboratory of Radio Frequency Heterogeneous Integration, Shenzhen University, Shenzhen 518060, China
[2]Shenzhen Key Laboratory of Ultrafast Laser Micro/Nano Manufacturing, Key Laboratory of Optoelectronic Devices and Systems of Ministry of Education/Guangdong Province, College of Physics and Optoelectronic Engineering, Shenzhen University, Shenzhen 518060, China
[3]Guangdong Laboratory of Artificial Intelligence and Digital Economy (SZ), Shenzhen 518107, China
*fucailing@szu.edu.cn

Received 20 July 2023; revised 4 August 2023; accepted 4 August 2023; posted 7 August 2023; published 21 August 2023

**We demonstrated a long-range and centimeter-spatial-resolution optical frequency domain reflectometry (OFDR) system based on an ultra-linear broadband optical frequency sweep. The high nonlinear sweeping effect of the distributed feedback (DFB) diode laser was suppressed by a pre-distortion method, ensuring that the injection-locking process remained stable during fast tuning over a large span. An optical linear frequency sweep (LFS) with a sweep range and sweep rate of up to 60 GHz and 15 THz/s, respectively, was ultimately obtained by optimizing the injection-locking system. The high performance OFDR based on the proposed LFS achieved a sampling spatial resolution of 1.71 mm. Furthermore, distributed strain sensing was implemented with high-spatial resolutions of about 5 cm and 7 cm in the measurement range over 1 km and 2 km, respectively.** 

https://doi.org/10.1364/OL.501034

Optical linear frequency sweeps (LFSs) are widely used in optical frequency domain reflectometry (OFDR) [1]. The spatial resolution and measurement distance of OFDR is directly dependent on the sweep range, sweep speed, and linearity of the LFS used. Currently, the OFDR based on an LFS with a sweep range of tens of nm generated by commercially tunable laser intracavity mirrors can achieve submillimeter spatial resolution distributed sensing [2]. However, the measurement distance and accuracy of OFDR are greatly limited by the high nonlinearity and severe phase noise of the LFS. On one hand, an auxiliary interferometer was previously introduced to synchronously monitor the noise generated by the LFS and eliminate it using a resampling algorithm [3,4], but the measurement distance was still limited to several tens of meters. On the other hand, LFS with high linearity has been achieved in a short period of time by using a swept electrical radio frequency (RF) signal to drive a modulator [5–7]. The obtained LFS has been used in OFDR to achieve recognition of Fresnel reflection events within a kilometer measurement range [8]. Moreover, distributed acoustic sensing with a spatial resolution of 28.4 cm was achieved using an LFS with a sweep range of 9 GHz generated by an in-phase and quadrature modulator [9]. But the narrow sweep range not only limited the spatial resolution, but also the maximum strain measurement range [10]. To achieve a wider sweep range, sideband injection-locking technology has been proposed to generate higher frequency RF [11] and an LFS with a sweep range of 15 GHz was achieved based on the 5th-order sideband [12]. The sweep range was further expanded to 25 GHz based on a higher-order sideband generated by high-power RF stimulation [13]. However, the inherent high nonlinearity of the distributed feedback (DFB) diode laser was not compensated for in the aforementioned LFS generating approach. This would raise the optical frequency deviation between the sideband and the slave laser and exceed the slave laser's locking range, making it difficult to obtain an LFS with a wider sweep range. In addition, optical phase-locked loop technology was also used to generate an LFS [14] and has been applied to link loss monitoring in long-range OFDR [15,16].

In this Letter, an injection-locking system for generating an ultra-linear broadband optical frequency sweep with a sweep range and sweep rate of 60 GHz and 15 THz/s, respectively, is proposed and demonstrated, where the side mode suppression ratio is over 21 dB. The nonlinear effect during the slave laser sweep process is effectively suppressed by using the proposed pre-distortion method, ensuring that the slave laser frequency could closely follow one of the high-order modulation sidebands of the main laser and achieve locking over a wide sweep range. The locking results under different tuning ranges with and without pre-distortion operations are compared. The performance of the obtained LFS is further verified in OFDR, including reflection identification events and distributed strain sensing.

An experimental setup was developed to generate an ultra-linear broadband optical frequency sweep using high-order sideband injection-locking technology, as shown in Fig. 1. The continuous wave light with a frequency of $f_1$ and a linewidth of 1 kHz generated by a fiber laser, Laser1 (main laser), as illustrated in the a-point spectrum in Fig. 1, is modulated by an intensity electro-optic modulator (EOM), where the working point of the EOM is controlled by a bias voltage controller. The RF signal

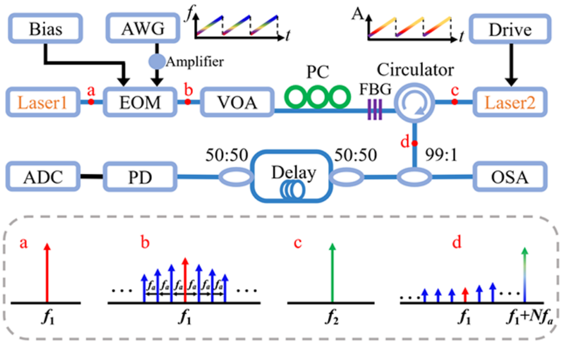


**Fig. 1.** Experimental setup to generate an ultra-linear broadband optical frequency sweep using high-order sideband injection-locking. AWG: arbitrary waveform generator; EOM: electro-optic modulator; VOA: variable optical attenuator; PC: polarization controller; FBG: fiber Bragg grating; ADC: analog-to-digital converter; PD: photodetector; OSA: optical spectrum analyzer. Note that $f_1$ and $f_2$ are the frequency of Laser1 (i.e., the main laser) and Laser2 (i.e., the slave laser), respectively. $f_a$ and $f_1+Nf_a$ are the RF frequency of the AWG and optical frequency of $N$th-order sideband, respectively.

with a frequency of $f_a$ output from an arbitrary waveform generator (AWG) is amplified by an amplifier and used to drive the EOM. In this way, higher-order sidebands could be generated on both sides of the frequency of Laser1, i.e., $f_1$, as shown in the b-point spectrum in Fig. 1. Then the frequency of the $N$th-order sideband could be expressed as $f_1 \pm Nf_a$, where the power is adjusted by a variable optical attenuator (VOA). To improve injection efficiency, a polarization controller (PC) and a fiber Bragg grating (FBG) are employed to adjust the polarization state and filter out the carrier of the high-order sideband spectrum before injecting a DFB laser, Laser2 (slave laser), via a circulator. The output frequency and linewidth of Laser2 is $f_2$ and 3 MHz, respectively, as illustrated in the c-point spectrum in Fig. 1, where the frequency could be tuned by adjusting the driving current. When the frequency of Laser2, i.e., $f_2$, is equal or close to the frequency of the $N$th-order sideband, i.e., $f_1 \pm Nf_a$, the frequency of Laser2 would be locked by the $N$th-order sideband and amplified, as shown in the d-point spectrum in Fig. 1. When a linear chirped signal with a sweep range of $\Delta f_a$ is output by the AWG, the frequency of the $N$th-order sideband would also change linearly. In this way, an optical LFS signal with a sweep range of $N\Delta f_a$, i.e., $F = N\Delta f_a$, will be generated. Note that the linewidth of the obtained LFS is determined by Laser1. Finally, the obtained LFS is divided into two parts by a 1:99 coupler. One part enters an optical spectrum analyzer (OSA) to measure the spectrum, while the other part enters a Mach–Zehnder interferometer (MZI) to generate the beat signal. The beat signal is photoelectrically converted by a photodetector (PD) and then collected by an analog-to-digital converter (ADC), which is finally used to monitor the locking status and calculate the instantaneous optical frequency (IOF), i.e., $\xi$.

To obtain an LFS with a wider sweep range, the deviation between $f_2$ and $f_1 \pm Nf_a$ should always be maintained within the locked range. Therefore, the frequency of Laser2, i.e., $f_2$, should be linearly adjusted synchronously with a linear chirped signal output by the AWG. However, a DFB laser under linear driving voltage exhibits an inherent high nonlinearity during high-speed sweeping, resulting in injection-locking failure. Therefore, an effective voltage pre-distortion method was proposed to solve

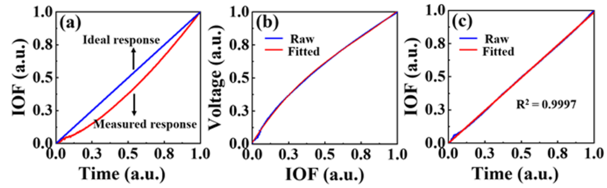


**Fig. 2.** (a) Ideal and measured IOF of Laser2 driven by a linear voltage. (b) Exchanged horizontal and vertical coordinates of the measured response curve in (a) and performed polynomial fitting on the raw data. (c) Measured IOF of Laser2 driven by the pre-distorted voltage and its linear fitting result.

the problem. A linear driving voltage of $V(t)$ was input to Laser2, and then the MZI with a delay length of about 0.2 m was used to measure the beat signal generated during the Laser2 sweeping and obtain the IOF by performing a Hilbert transform. As shown in Fig. 2(a), an obvious frequency deviation between the ideal (blue line) and measured IOF (red curve) occurred. Clearly, the function between the IOF and time, i.e., $\xi(t)$, was nonlinear, and could be equivalently represented as $\xi(V)$. To obtain the relationship between the driving voltage, i.e., $V$, and IOF, i.e., $\xi$, the horizontal and vertical coordinates of the previously measured $\xi(V)$ was exchanged, as shown by the blue line in Fig. 2(b). Then a polynomial fitting was performed to obtain a fitting function, i.e., $V(\xi)$, as shown by the red curve in Fig. 2(b). When the linear independent variables were $\xi_1$, $\xi_2, \ldots\ \xi_{n-1}$, $\xi_n$, the corresponding pre-distortion voltage, i.e., $V_1$, $V_2, \ldots\ V_{n-1}$, $V_n$, could be calculated based on the obtained function of $V(\xi)$. Finally, the IOF of Laser2 was corrected to linear using the calculated pre-distortion voltage. Similarly, the IOF of Laser2 driven by the obtained pre-distortion voltage was measured again. As shown in Fig. 2(c), the measured IOF agreed well with the linear fitting, where the linear fitting coefficient was 0.9997. This indicated that the linearity of the measured IOF was significantly improved.

To further demonstrate the effectiveness of the voltage pre-distortion method for stable injection-locking to generate the broadband LFS, a high-order sideband injection-locking experiment was conducted. The output wavelength and power of Laser1 in the injection-locking experiment were 1549.7 nm and 13 dBm, respectively. Three linear chirp RF signals with a chirp time of 4 ms and different sweep ranges $\Delta f_a$ of 6, 9, and 15 GHz were generated by the AWG. Then the 4th-order ($N = 4$) sideband was locked, corresponding to sweep ranges $N\Delta f_a$ of 24, 36, and 60 GHz. In the experiment, the length of the delay fiber was 81 m, which was larger than the theoretical coherence length of Laser2, but much smaller than that of Laser1. The LFS obtained by locking the 4th-order sideband would generate a sinusoidal beat signal in a stable locking state. But for the unlocking state, the sweep light of Laser2 generated by the driving voltage would occupy the main component of the spectrum, leading to interference failure. The beat signals were investigated, when three types of driving voltages illustrated in Fig. 3—i.e., linear sawtooth voltage without pre-distortion, pre-distortion voltage, and pre-distortion—combined with a return voltage were employed for Laser2. The return time was equal to the linear chirp time of 4 ms for the AWG. Note that the return voltage (blue square section) between two adjacent sweeping cycles was used to solve the delay response generated by Laser2 during high-speed sweeping. When the sweep range was 24 GHz, the locking failure, i.e.,

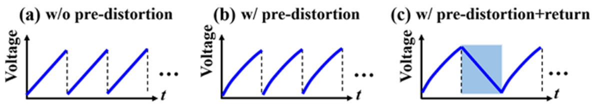


**Fig. 3.** Three types of driven voltages for Laser2: (a) linear sawtooth voltage without pre-distortion; (b) pre-distortion voltage; and (c) pre-distortion combined with return voltage.

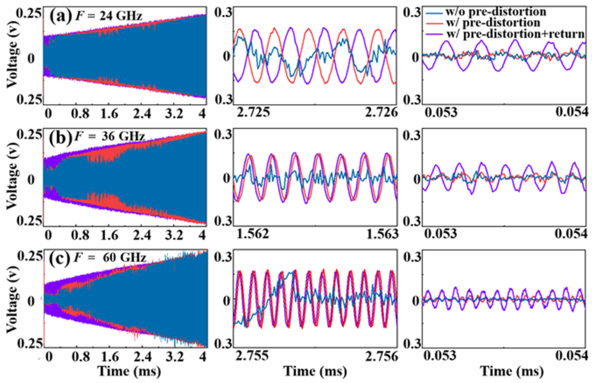


**Fig. 4.** Generated beat signals under the three driving types of voltages in Fig. 3 when the sweep ranges of high-order sideband injection-locking were (a) 24 GHz, (b) 36 GHz, and (c) 60 GHz, respectively.

the interference failure, could be observed between 2.725 and 2.726 ms under a linear sawtooth voltage without pre-distortion, as shown by the blue curve in Fig. 4(a). Fortunately, the pre-distortion voltage signals could be stably locked and generated beat signals under a pre-distortion voltage and pre-distortion combined with return voltage, as shown, respectively, by the red and purple curves in Fig. 4(a). However, in the initial section, such as between 0.053 and 0.054 ms, the 4th-order sideband was only locked under a pre-distortion combined with return voltage, as shown by the purple curve in Fig. 4(a). When the sweep ranges were increased to 36 and 60 GHz, the same results were exhibited, as shown in Figs. 4(b) and 4(c).

In addition, the spectra of the LFS with a sweep range of 60 GHz obtained by injection-locking using the driving voltage in Fig. 3(c), are shown in Fig. 5(a), and the spectra of the LFS with and without the FBG in Fig. 1 were further compared. As shown in Fig. 5(a), the carrier and unwanted sidebands could be effectively filtered out without affecting the power of the LFS through the FBG, and the side mode suppression ratio was greater than 21 dB. Subsequently, the IOF of the obtained LFS was also calculated. As shown in Fig. 5(b), the frequency range and linear fitting slope were 60 GHz and 15 THz/s, respectively,

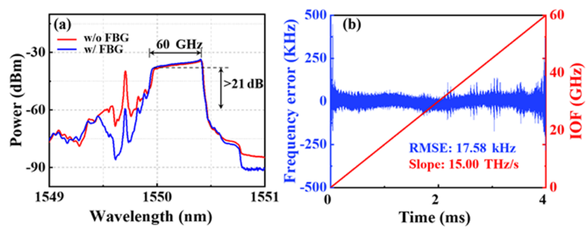


**Fig. 5.** (a) Measured LFS spectrum with and without FBG in Fig. 1, where the sweep range was 60 GHz. (b) Calculated IOF (right axis) and frequency error (left axis) of the LFS after the FBG filtering. The RMSE of the frequency error was 17.58 kHz.

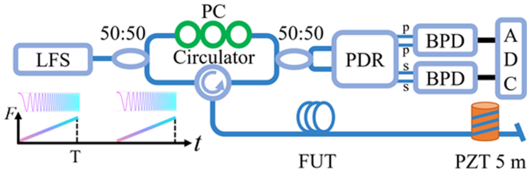


**Fig. 6.** Experimental setup for OFDR distributed strain sensing based on previously obtained LFS with pre-distortion combined with return voltage and FBG, where the LFS range and the rate were 60 GHz and 15 THz/s, respectively. PDR: polarization diversity receiver; BPD: balanced photodetector; FUT: fiber under test; PZT: piezoelectric transducer.

which were consistent with the theoretical value, and the root mean square error (RMSE) of the sweep error was only 17.58 kHz. This indicated that an ultra-linear broadband optical frequency sweep with a sweep range and sweep rate of 60 GHz and 15 THz/s, respectively, has been achieved by optimizing the injection-locking system through pre-distortion combined with return voltage and the FBG. In the future, an EOM with higher RF input power can be further selected to generate higher-order sidebands to increase the amplification factor of the LFS sweep range and reduce the requirement for an AWG.

To further verify the performance of the obtained LFS, a distributed strain sensing based on OFDR was carried out. As shown in Fig. 6, the previously obtained LFS is divided into two parts via a coupler. One part enters the reference arm as the reference signal, while the other part enters a fiber under test (FUT), i.e., single-mode fiber (SMF), via a circulator as the detection signal. The polarization adjustment is achieved by a PC. The Rayleigh backscattering from the FUT is mixed with the reference signal and sent to the polarization diversity receiver (PDR), which is then detected by a pair of balanced photodetectors (BPDs). An ADC with a sampling rate of 1 GHz/s is used to acquire photocurrent signals. Firstly, the reflection peaks of three fiber connectors, i.e., $APC_1$, $APC_2$, and $APC_3$, located at positions of 1003, 2013, and 2020 m, respectively, were measured where the length of the FUT was 2045 m, as shown in Fig. 7(d). As shown in Figs. 7(a)–7(c), the 3dB-bandwidth spatial resolution remained at 1.71 mm regardless of the position of the connectors. The measured spatial resolution was consistent with the theoretical spatial resolution calculated by $c/2nF$, where $c$ is the velocity of light in a vacuum, $n$ is the refractive

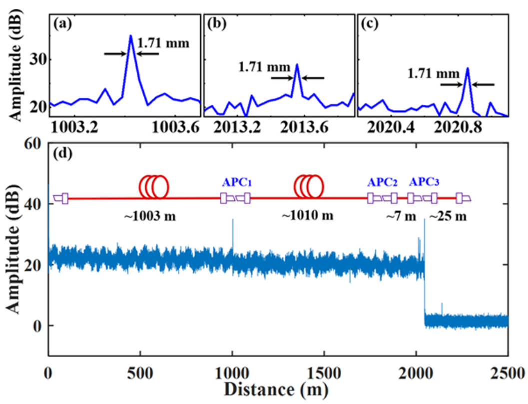


**Fig. 7.** Measured reflection peaks of (a) $APC_1$, (b) $APC_2$, and (c) $APC_3$ connectors located at positions of 1003, 2013, and 2020 m, respectively; (d) measured reflection trace of the FUT with a length of 2045 m.

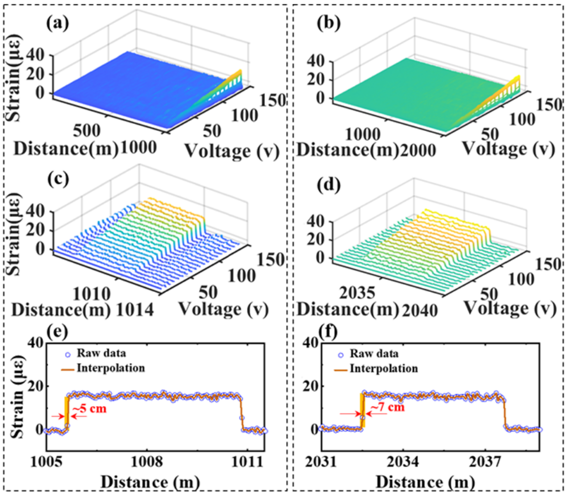


**Fig. 8.** Demodulated strain distribution under different driving voltages, when the PZT was connected to the far end of the (a) 1-km, and (b) 2-km FUTs, respectively; (c) and (d) enlarged views of (a) and (b), respectively, in the PZT area; (e) and (f) strain distribution at a driving voltage of 135 V for the 1-km and 2-km-long FUTs, respectively.

index of the medium, and $F$ is the sweep range of the LFS, i.e., 60 GHz. Subsequently, a commercial piezoelectric transducer (PZT) wrapped with a 5-m-long SMF was connected to the far end of the 1-km and 2-km FUT, respectively. The driving voltage for the PZT was increased from 0 to 135 V in steps of 7.5 V to generate a strain field. As shown in Figs. 8(a) and 8(c), when the PZT was placed at the far end of the over 1-km-long FUT, the strain distribution under different driving voltages could be well identified based on the proposed ultra-linear broadband optical frequency sweep OFDR system, and only slight fluctuations could be observed in the strain-free region. Similarly, the strain distribution applied by the PZT could also be successfully demodulated for the over 2-km-long FUT, as illustrated in Figs. 8(b) and 8(d). As shown in Figs. 8(e) and 8(f), the spatial resolutions, i.e., the rising edges (10–90%), at a driving voltage of 135 V for the 1-km and 2-km-long FUTs were approximately 5 cm and 7 cm, respectively. Note that the above OFDR system did not use an auxiliary interferometer for phase noise compensation [6,17], nor did it perform multiple repeated acquisitions to average the signal. This indicated that the OFDR system based on the proposed LFS can achieve distributed strain sensing with centimeter-spatial-resolution within a range of 2 km without tedious post-processing calculations. The OFDR system exhibits attractive prospects in real-time online processing due to the excellent sweep performance of the proposed LFS.

In conclusion, we demonstrated an ultra-linear broadband optical frequency sweep by using a high-order sideband injection-locking technique. An MZI was used to monitor the IOF of the DFB Laser2 under current modulation. Combined with the proposed pre-distortion method, a fast broadband optical LFS with a sweep range and sweep rate of 60 GHz and 15 THz/s, respectively, achieved a frequency error of only 17.58 kHz. Three fiber connectors, $APC_1$, $APC_2$, and $APC_3$, located at positions of 1003, 2013, and 2020 m, respectively, were successfully identified with a spatial resolution of 1.71 mm, equivalent to the theoretical spatial resolution. Furthermore, the OFDR based on the proposed LFS achieved distributed strain sensing with high-spatial resolutions of about 5 cm and 7 cm in measurement ranges over 1 km and 2 km, respectively, without the use of post-processing procedures, such as phase noise compensation and multiple averaging. The proposed long-range and centimeter-spatial-resolution OFDR has attractive prospects for health monitoring of aircraft wings and other structures.

**Funding.** National Key Research and Development Program of China (2022YFE0111400); National Natural Science Foundation of China (U1913212, U22A2088); Guangdong Science Technology Department (2021A1515011925); Shenzhen Science and Technology Program (JCYJ20200109114020865, JCYJ20200109114201731, JCYJ20200810121618001, JSGG20201102152200001); Shenzhen Key Laboratory of Ultrafast Laser Micro/Nano Manufacturing (ZDSYS20220606100405013); Shenzhen Key Laboratory of Photonic Devices and Sensing Systems for Internet of Things..

**Disclosures.** The authors declare no conflicts of interest.

**Data availability.** Data underlying the results presented in this Letter are not publicly available at this time but may be obtained from the authors upon reasonable request.

## REFERENCES

1. Z. Ding, C. Wang, K. Liu, J. Jiang, D. Yang, G. Pan, Z. Pu, and T. Liu, Sensors **18**, 1072 (2018).
2. Y. Meng, C. Fu, L. Chen, C. Du, H. Zhong, Y. Wang, J. He, and W. Bao, Opt. Lett. **47**, 6289 (2022).
3. E. D. Moore and R. R. McLeod, Opt. Express **16**, 13139 (2008).
4. T. J. Ahn, J. Y. Lee, and D. Y. Kim, Appl. Opt. **44**, 7630 (2005).
5. S. Ohno, D. Iida, K. Toge, and T. Manabe, Opt. Express **24**, 19651 (2016).
6. X. Fan, Y. Koshikiya, and F. Ito, Opt. Lett. **32**, 3227 (2007).
7. D. Chen, Q. Liu, and Z. He, Opt. Express **26**, 16138 (2018).
8. Z. Zhang, X. Fan, M. Wu, and Z. He, J. Lightwave Technol. **37**, 2634 (2019).
9. J. Xiong, Z. Wang, J. Jiang, B. Han, and Y. Rao, Opt. Lett. **46**, 2569 (2021).
10. Z. Zhang, X. Fan, and Z. He, J. Lightwave Technol. **37**, 4590 (2019).
11. G. J. Schneider, J. A. Murakowski, C. A. Schuetz, S. Shi, and D. W. Prather, Nat. Photonics **7**, 118 (2013).
12. F. Wei, B. Lu, J. Wang, D. Xu, Z. Pan, D. Chen, H. Cai, and R. Qu, Opt. Express **23**, 4970 (2015).
13. B. Wang, X. Fan, S. Wang, J. Du, and Z. He, Opt. Express **25**, 3514 (2017).
14. G. Gorju, A. Jucha, A. Jain, V. Crozatier, I. Lorgeré, J.-L. Le Gouët, F. Bretenaker, and M. Colice, Opt. Lett. **32**, 484 (2007).
15. Y. Feng, W. Xie, Y. Meng, L. Zhang, Z. Liu, W. Wei, and Y. Dong, J. Lightwave Technol. **38**, 6227 (2020).
16. Y. Meng, W. Xie, Y. Feng, J. Yang, L. Zhang, Y. Bai, W. Wei, and Y. Dong, IEEE Photonics J. **13**, 7100307 (2021).
17. Z. Ding, X. S. Yao, T. Liu, Y. Du, K. Liu, J. Jiang, Z. Meng, and H. Chen, Opt. Express **21**, 3826 (2013).